Flowfield Scaling in Sharp Fin-Induced Shock Wave/Turbulent Boundary-Layer Interaction

D.S. Dolling* and W.B. McClure†
Princeton University, Princeton, New Jersey

This paper presents the results of an experimental investigation of the three-dimensional interaction of a swept planar shock wave with a turbulent boundary layer. The shock wave was generated by a sharp, unswept fin mounted normal to a flat test surface. On the two test surfaces used, the incoming boundary layers varied in thickness by 3:1. In both cases, the freestream Mach number was nominally 3, the freestream Reynolds number 6.3×10^7 m^{-1}, and the wall temperature close to adiabatic. Detailed yaw angle and pitot pressure surveys in the two cases reveal a similar flowfield structure that can be correlated using a simple scaling technique.

Nomenclature

a, b = exponents in scaling law, Eq. (1)
C_f = skin-friction coefficient
L_s = distance along the shock wave measured from the fin leading edge
L_u = streamwise upstream influence
L_{u_n} = upstream influence normal to the shock wave
M = Mach number
P_0 = stagnation pressure
Pt = pitot pressure
Re_{δ_0} = Reynolds number based on δ_0
α = fin angle of attack
β = flow yaw angle (measured relative to the incoming freestream in a plane parallel to the test surface)
δ_0 = local incoming boundary-layer thickness
δ^* = boundary-layer displacement thickness
θ = boundary-layer momentum deficit thickness

Subscripts

∞ = freestream conditions
n = normal to shock wave
w = at the wall
2 = downstream of the shock wave

Introduction

IN Ref. 1 the spanwise growth of upstream influence was measured in a three-dimensional (3-D), sharp fin-induced shock wave/turbulent boundary-layer interaction. The fin was mounted normal to the test surface, was effectively "semi-infinite" in height, and had an unswept leading edge. A planview sketch of the model and coordinate system (the same as used in the current study) is shown in Fig. 1. Tests were made on the wind tunnel floor and on a horizontal flat plate with a sharp leading edge. In all cases the freestream Mach number M_∞ was nominally 3 and the wall temperature approximately adiabatic.

A scaling method, originally developed for use in swept compression ramp flows,[2] was modified and used to correlate the data.[1,3] The functional form of the correlation curve is given by

$$\frac{L_{u_n}}{\delta_0} Re_{\delta_0}^a f(M_n) = g\left(\frac{L_s}{\delta_0} Re_{\delta_0}^b\right) \tag{1}$$

where L_{u_n} is the upstream influence normal to the shock wave, δ_0 the local incoming boundary-layer thickness, Re the Reynolds number, M_n the Mach number normal to the shock wave, L_s the distance along the shock wave measured from the fin leading edge, and a and b the empirically derived constants. A good correlation was obtained with $a = b = \frac{1}{3}$ (the same values as in Ref. 2). Over the limited range of angles of attack that were tested (1 deg $\leq \alpha \leq$ 14 deg), the dependence on M_n was weak, with $f(M_n) = 1/M_n$ giving a good correlation. In addition to being valid in sharp fin and swept compression ramp flows, recent tests[4,5] have shown that Eq. (1) is also applicable to interactions generated by swept-back, sharp fins.

Equation (1) can be rewritten in abbreviated form as

$$L'_{u_n} = g(L'_s) \tag{2}$$

where the prime indicates the nondimensional form given above. The success of this rather simple approach raised the question of whether it would also apply to dimensions associated with features and details in the flowfield above the test surface. Although detailed flowfield surveys have been made in similar interactions,[6,7] they were obtained at a single test condition, thus the scaling question could not be addressed. The objective of the present tests was to investigate the latter and, at the same time, hopefully learn more about the flowfield structure. To do this, detailed yaw angle and pitot surveys were made in two interactions: on the wind tunnel floor and on a flat plate. The results of these experiments are presented herein.

Experimental Program

Only a brief outline is given below. A full description of the probe drive mechanism and operation, data acquisition techniques, the calibration procedures, and the extensive interference studies carried out prior to the test program are given in Refs. 8 and 9.

Wind Tunnel

The experiments were carried out in the Princeton University 20×20 cm supersonic, high Reynolds number wind tunnel. This is a blowdown facility with a nominal freestream Mach number of 2.95. The settling chamber pressure and temperature were 6.8×10^5 Nm$^{-2} \pm 1\%$ and 265 K $\pm 5\%$,

Presented as Paper 83-1754 at The AIAA 16th Fluid and Plasma Dynamics Conference, Danvers, Mass., July 14-16, 1983; received June 24, 1983; revision received March 6, 1984.

*Research Engineer, Mechanical and Aerospace Engineering Department; currently, Asst. Professor, Department of Aerospace Engineering and Engineering Mechanics, The University of Texas at Austin, Texas. Senior Member AIAA.

†Graduate Student, Mechanical and Aerospace Engineering Department; currently with USAF, ASD/ENFTA, Wright-Patterson AFB, Ohio.

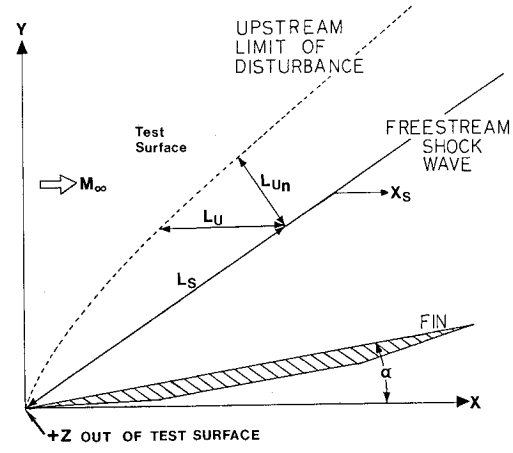

Fig. 1 Model and coordinate system.

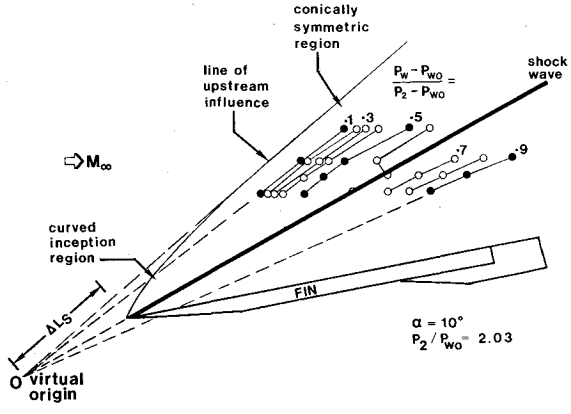

Fig. 2 Conically symmetric and inception regimes of the flowfield.

respectively, giving a nominal freestream Reynolds number of 6.3×10^7 m^{-1}. The wall temperature was close to adiabatic for all tests.

Models

Two similar configurations were used. In both, a 29.2-cm long, 1.27-cm thick aluminum fin with a sharp unswept leading edge was mounted perpendicular to a flat test surface on which the incoming boundary layer developed (Fig. 1). In case 1, the test surface was the tunnel floor; in case 2, it was a flat plate with a sharp leading edge that spanned the tunnel horizontally. All tests were carried out at $\alpha = 10$ deg. Although neither fin spanned the tunnel, each fin's height (14 cm in case 1 and 8.9 cm in case 2) was experimentally confirmed to be effectively semi-infinite. This was done by reducing the height and repeating surveys. In each case the data fell within the expected error band and no systematic changes were observed.

Surface Properties

Surface data were obtained using two methods: 1) static pressure distributions were measured along spanwise rows of pressure orifices aligned with the X direction, and 2) surface flow angles were obtained from kerosene-lampblack streak patterns. The latter technique is described in Ref. 10.

Flowfield Properties

A computer-controlled nulling cobra probe was used to measure flow yaw angle β and pitot pressure Pt simultaneously. Surveys were made at 20 stations in one X-Z plane for each case. The Y coordinate of each plane was chosen such that it intersected the shock wave at the same value of L_s'. The overall accuracy of the yaw angle measurement is estimated to be approximately 1 deg, while that of the probe tip position is estimated to be ± 0.02 cm in both the X and Y directions.

Table 1 Incoming properties at the fin leading edge

	δ_0, cm	δ^*, cm	θ, cm	C_f
Case 1	1.25	0.34	0.07	0.00119
Case 2	0.50	0.16	0.03	0.00136

Table 2 Locations of survey lines

	Y, cm	L_s, cm	L_s'	L_u, cm
Case 1	12.1	26.9	1650	9.3
Case 2	6.4	13.6	1640	4.8

Incoming Boundary Layers

The incoming boundary layers on both test surfaces have been surveyed extensively, are two-dimensional, and fit the wall-wake law well.[2,11] The incoming properties (at the fin leading edge) are tabulated in Table 1. Due to the sweep of the shock wave, the local incoming properties along the line of upstream influence are a function of spanwise position. At the two survey planes $\delta_0 = 1.55$ cm for case 1 and 0.59 cm for case 2. These are the values used in Figs. 3-8.

Results and Discussion

Surface Properties

As noted in several other studies (i.e., Refs. 4-7 and 12-14), the interaction footprint is conically symmetric outside of an initial curved "inception" region. "Conically symmetric" means that surface features lie along rays that intersect the trace of the inviscid shock wave at a common origin. Figure 2, which shows isobars and the line of upstream influence for test case 1, confirms this and delineates the two flow regimes. In this instance, the origin is not at the leading edge of the fin but is displaced from it by distance ΔL_s along the trace of the shock wave. The shock wave location, in this and subsequent figures, was calculated taking $M_\infty = 2.95$ and $\alpha = 10$ deg.

Flowfield Surveys

The locations of the two survey lines are given in Table 2. The difference in physical scale between the two flows can be judged from the values of L_u in the right-hand column. Surveys were started upstream of the interaction, progressing downstream in increments in $X \leq 0.8$ cm, with closer spacing in the vicinity of the shock wave. The constraints of tunnel size and fin proximity prevented measurements from being made far enough downstream to locate the "end" of the interaction where the yaw angle, β, is constant and equal to α. At the last station of case 2, however, the variation in $\beta(Z)$ was only 2 deg.

Results from previous work indicate that the normalized streamwise interaction length scale should be the same in both cases. Because the spanwise locations of the surveys did not coincide with rows of pressure orifices, this could not be checked directly. However, the normalized upstream influence was checked using the kerosene-lampblack streak patterns. The values of L_u' were 580 and 590 in cases 1 and 2, respectively.

Yaw angle and pitot pressure profiles at nine stations for case 1 are shown in Figs. 3 and 4. For clarity, adjacent profiles in Fig. 4 have been plotted using different symbols. Pt is normalized by $Pt_{2\infty}$, the undisturbed freestream value. Thus, in the inviscid flow upstream and downstream of the shock wave, the theoretical values of $Pt/Pt_{2\infty}$ are 1.0 and 1.44, respectively. The measured values at the top of the surveys at stations 1, 8, and 9 are within 1.5% of these values. The solid

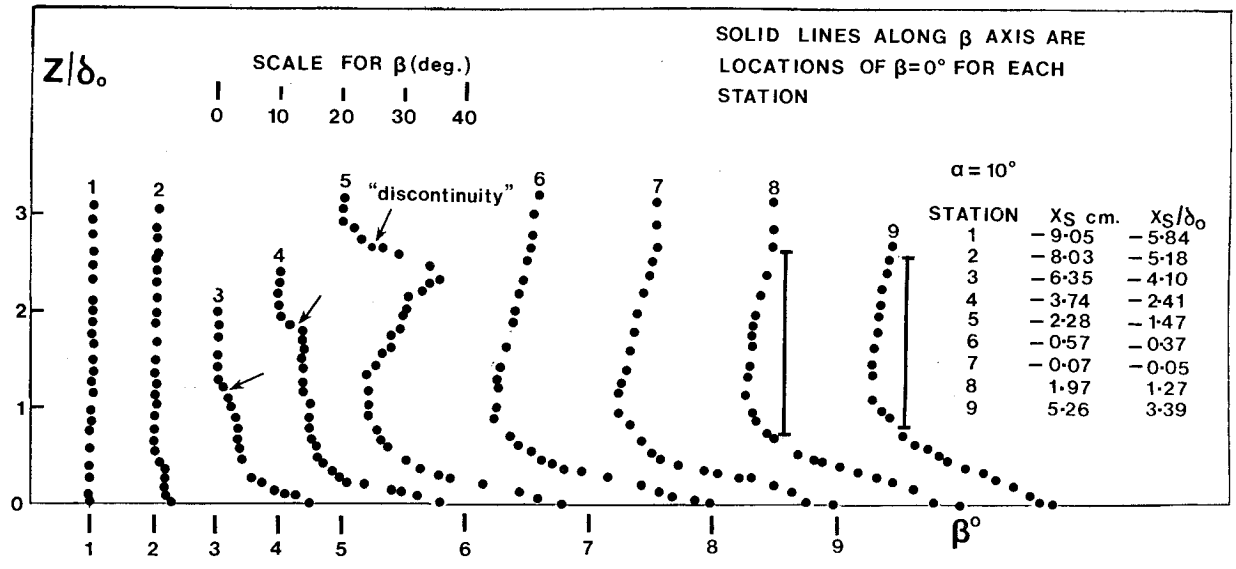

Fig. 3 Yaw angle surveys (case 1).

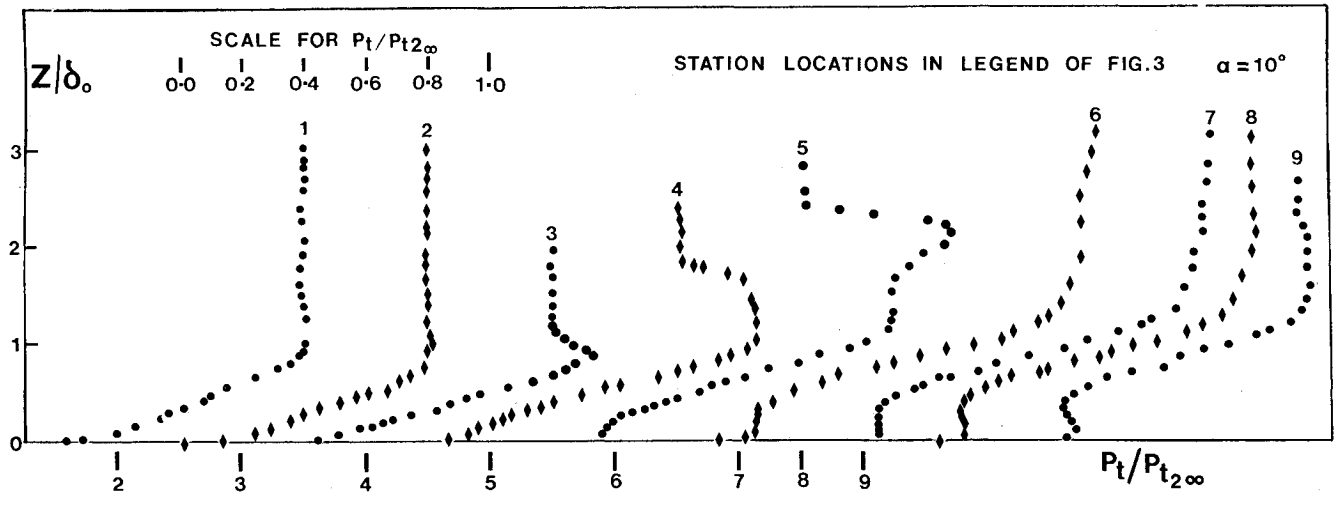

Fig. 4 Pitot pressure surveys (case 1).

bars along the horizontal axes are the locations $\beta = 0$, $Pt/Pt_{2\infty} = 0$ for profiles 1-9, respectively. In the description of the profile development, distances relative to the shock wave and normal to the test surface are given in terms of δ_0. This is solely for the convenience of avoiding dimensional scales, and does not imply that δ_0 alone is the appropriate scaling parameter.

Many of the features of both the pitot pressure and yaw angle profiles have been noted in previous studies[6,7,15] and, hence, will only be described briefly herein. The surveys at stations 1-4 show the inception of the interaction flowfield. Yaw angles at the surface increase rapidly from 0 deg at station 1 to 32 deg at station 4. Above the test surface, discontinuities are observed in both the yaw angle and pitot pressure profiles at stations 3 and 4. This is indicative of the coalescence of compression waves.

At station 5, a new development occurs which was not observed in the earlier work of Oskam et al.[6,7] or Peake,[15] nor in numerical simulations of this flowfield.[16,17] Near the wall, both yaw and pitot profiles are similar to those upstream, although the beginnings of a region of constant pressure are noticeable. Again, β decreases to ~ 5 deg at $Z \sim 0.8\ \delta_0$, remains constant over a short distance, but then increases rapidly to a maximum of 16 deg before returning to 0 deg at $Z \sim 2.9\ \delta_0$. Corresponding to this local maximum in β is a sharp overshoot in the pitot profile, to a value of 1.7, followed by a rapid return to the undisturbed value of 1.0. The "discontinuity" in β, observed at the upstream stations, also occurs at $Z \sim 2.7\ \delta_0$. Due to the proximity of the shock wave, these large angles were originally thought to be caused by probe interference. Tests made with the probe entering through the tunnel ceiling yielded the same result, thus discounting this possibility. Furthermore, tests made using a fin with a reduced height also gave the same result, eliminating the possibility of finite height effects.

Closer to the theoretical shock wave position, at stations 6 and 7, β at the wall has increased to 40 deg. In the region of rapidly decreasing β, close to the wall, the pitot pressure is almost constant. Again, β decreases to ~ 5 deg at $Z \sim 0.8\ \delta_0$, then increases gradually. At the maximum Z in profile 6, $\beta = 12$ deg and is still increasing, as is the pitot pressure. The precise position of station 7 is not absolutely certain. It is theoretically very close to, but upstream of, the calculated shock wave, but the results suggest that it may in fact be downstream of it. Near the maximum Z, β reaches a constant value of 10-11 deg, the theoretical value for stations downstream of the shock wave.

The behavior at station 6 was not observed in Oskam's study,[6,7] but can be seen in Peake's[15] profiles at $M_\infty = 2$ ($\alpha = 8$ deg) and at $M_\infty = 4$ ($\alpha = 8, 16$ deg). At the maximum

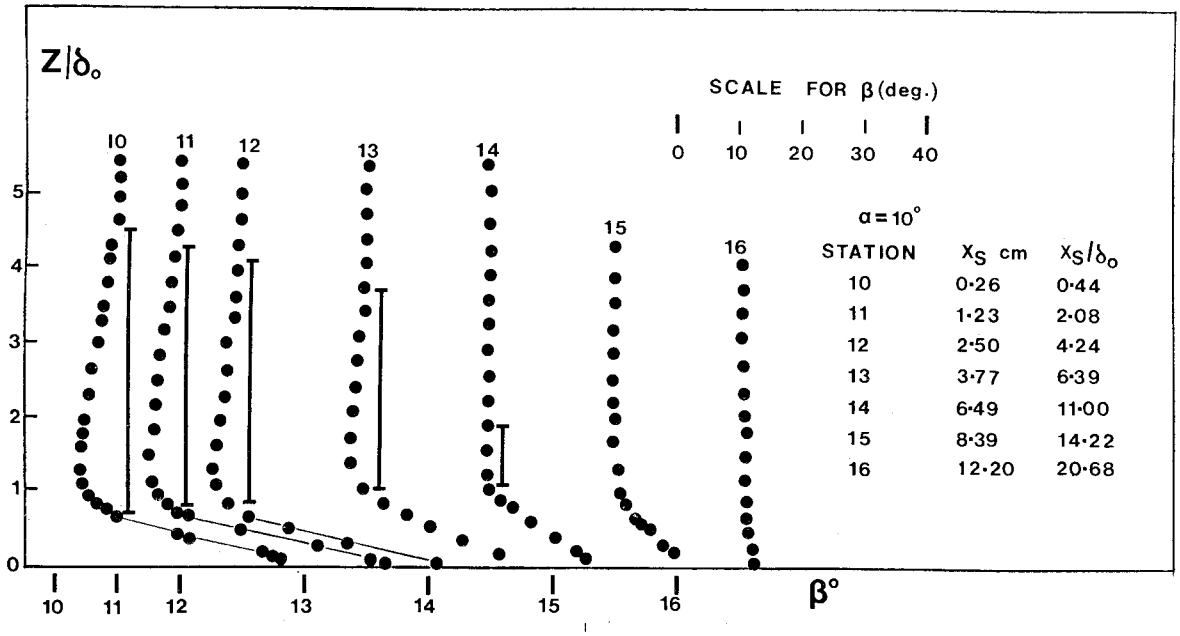

Fig. 5 Yaw angle surveys downstream of the shock wave (case 2).

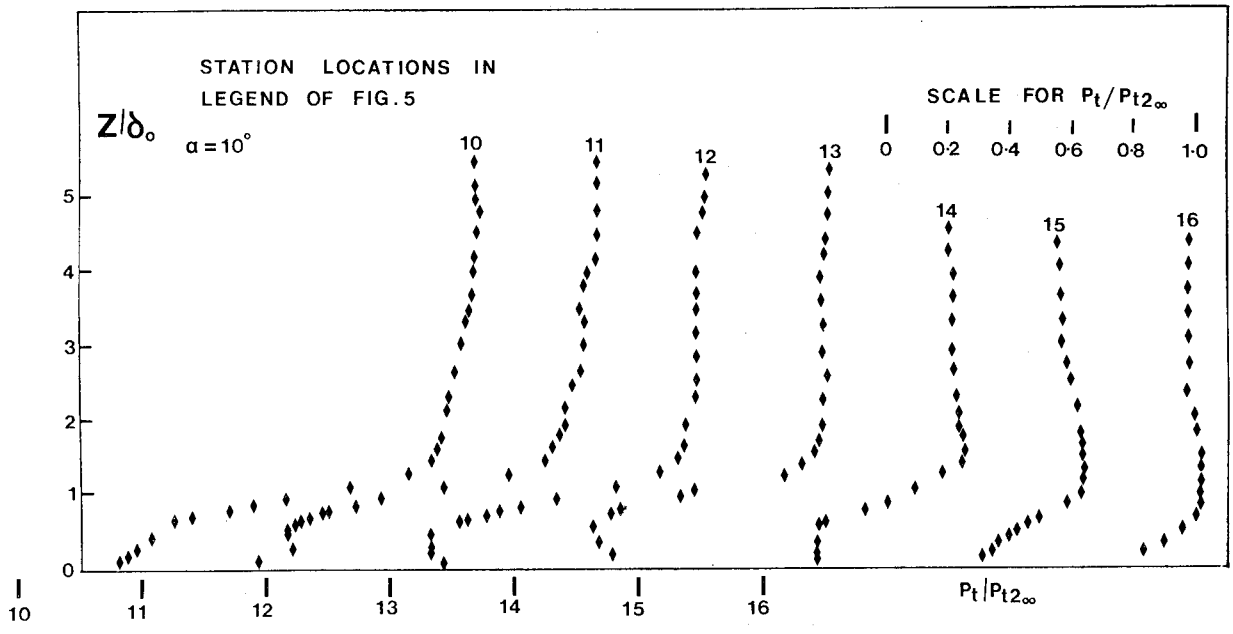

Fig. 6 Pitot pressure surveys downstream of the shock wave (case 2).

vertical position of Peake's probe (1.25-1.5 cm), β was still increasing. This suggests that the theoretical planar shock wave is not reached until a significant distance above the test surface.

At stations 8 and 9, both downstream of the shock wave, the yaw profile relaxes slowly to the downstream condition (i.e., a uniform profile with $\beta = 10$ deg). Although the theoretical angle of 10 deg is reached over the upper portion of the profiles, there is a relatively large region below it, indicated by a vertical bar, where $\beta < \alpha$ and the flow is turning in toward the fin.

As mentioned earlier, measurements were made further downstream of the shock wave (in dimensional and normalized terms) in case 2 than in case 1. The results are shown in Figs. 5 and 6. Note that the vertical scale is twice that of Figs. 3 and 4. The profiles at stations 10, 11, and 12 are in the same relative region as those at 8 and 9 for case 1. With increasing distance downstream, β at the wall steadily decreases, the region over which $\beta < \alpha$ decreases in size, and the region of constant pitot pressure near the wall starts to fill out. By station 14, the $\beta < \alpha$ region is barely detectable and by 15 has gone, as has the region of constant pitot pressure. At 16, the yaw angle profile is almost uniform and the pitot profile has the characteristic shape of a 2-D boundary layer.

Flowfield Scaling

The critical question is that of the appropriate parameter(s) for scaling the vertical axis. Two obvious choices for the vertical axis are 1) Z/δ_0 and 2) the nondimensional form of Eq. (1) [i.e., $(Z/\delta_0)Re_{\delta_0}{}^{\frac{1}{3}}$]. Both forms were examined and are discussed below.

Contour plots of yaw angle and pitot pressure, constructed from the complete set of surveys‡ and scaled according to Eq.

‡The complete data set, on magnetic tape or as hard copy, is available from the Gas Dynamics Laboratory.

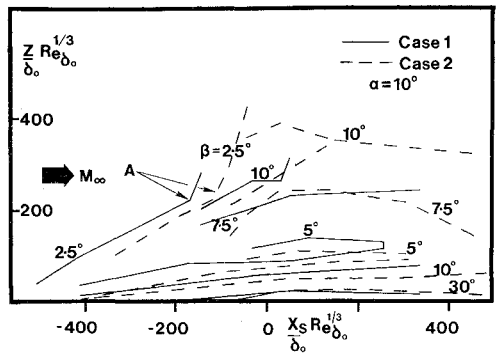

Fig. 7 Scaled yaw angle contours (cases 1 and 2).

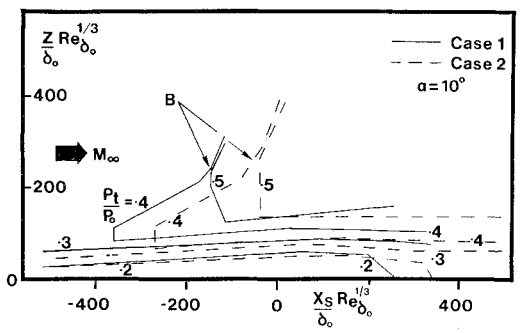

Fig. 8 Scaled pitot pressure contours (cases 1 and 2).

(2), are shown in Figs. 7 and 8. For clarity only five angle and four pressure contours are shown. The latter are normalized by the freestream stagnation pressure P_0. There were insufficient data to adequately document the region of large angles around station 5, thus it is not included. In Fig. 7, the flow angle above the upper 10-deg contour is equal to 10 deg everywhere. Also, the contour labeled 2.5 deg actually denotes the "discontinuity" mentioned earlier and represents a range where β is between 2 and 4 deg.

The 30-50 unit streamwise shift between the two sets of contours is most probably the cumulative result of several factors. First, there is the inaccuracy in locating where the shock wave actually crosses the survey plane. The absolute error increases with L_s and will be larger for case 1 than case 2. Second, the necessity of having a "deadband" in the probe nulling software contributes a further error. In regions where $d\beta/dZ$ is large, the error is estimated to be within the accuracy of the vertical measurement. In shallower gradients the error is more significant. Third, the scaling method is an approximate, practical means of correlating results at different test conditions and there will necessarily be scatter.

Except for this discrepancy, the two data sets compare favorably when scaled this way. In both cases, the 2.5-deg contour (delineating the "discontinuity") intersects the test surface at the upstream influence line, is at the same angle, and deviates from its quasilinear trend at the same normalized height. Similarly, the shapes of the 0.4 and 0.5 pitot contours are the same in both cases. In the vicinity of the wall, the details match well with the $\beta = 10$ deg and $\beta = 30$ deg contours starting at essentially the same position and following one another closely with distance downstream. The region downstream of the shock wave in which $\beta < \alpha$ is centered at the same height above the test surface. Furthermore, the 5-deg contour associated with this region terminates at about the same streamwise position. Finally, the position at which the pitot profile near the wall fills out occurs at the same streamwise station.

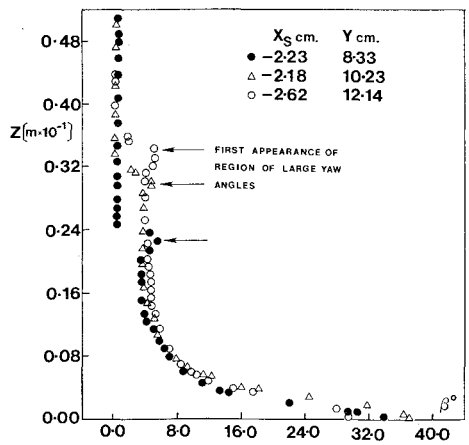

Fig. 9 Spanwise development of region of large yaw angles.

That Z/δ_0 is inappropriate for scaling the vertical axis can be seen directly from Figs. 7 and 8. If the vertical axis of these figures is replotted in terms of Z/δ_0 alone, then the vertical positions of the contours for the two cases will be shifted relative to one another by their ratio of $Re_{\delta_0}^{\frac{1}{3}}$. Since for case 1, $Re\delta_{0^3}^{\frac{1}{3}} \sim 100$ and for case 2, $Re\delta_{0^3}^{\frac{1}{3}} \sim 72$, then this shift will be in the ratio 7:10. Thus, for example, points such as "A" of Fig. 7 (which is where the 2.5-deg contours change slope) or points "B" of Fig. 8 (where the upstream and downstream contours given by $Pt/P_0 = 0.5$ merge) will be shifted apart in this ratio. Features within the boundary layer such as the $\beta = 30$-deg contour and the $Pt/P_0 = 0.2$ contour, which correlate well in the coordinate system of Fig. 7, will also be shifted apart.

Region of Large Yaw Angles Upstream of the Shock Wave

Just upstream of the shock wave, but at a significant distance above the test surface, Fig. 3 shows that large yaw angles occur. The same result was obtained in case 2. Because of 1) the larger physical scale of the flowfield, and 2) the flexibility of the probe-positioning mechanism, traverses were made at two other spanwise stations in case 1 to track this development. At the first, $Y = 10.2$ cm, five surveys were made to locate where the large angles first appeared. Based on these data and those along the main survey plane, one additional survey was made at $Y = 8.3$ cm.

The results indicate that this region exists at all spanwise stations, though at a progressively lower Z as the leading edge is approached (Fig. 9). A line drawn through the three points at which the region is first noticeable intersects the test surface at an angle of about 8 deg. Since the three points were closely spaced and are indicators of the onset of a region rather than of a well-defined change, this origin is only qualitative. What the data do show, is that, like other features of the flowfield, the spanwise development of this region is conical.

Concluding Remarks

An experimental study has been made of the three-dimensional shock wave/turbulent boundary-layer interaction generated by a sharp fin at angle of attack. The freestream Mach number was 2.95, the freestream Reynolds number 6.3×10^7 m^{-1}, and the wall temperature approximately adiabatic. Detailed yaw angle and pitot surveys were obtained in two flowfields in which the incoming turbulent boundary-layer thickness varied in the ratio 3:1. The objective of the study was to investigate the scaling of the flowfield. The results show that:

1) Outside of an initial curved inception zone, the interaction footprint is conically symmetric, as also shown in Ref. 4.

2) Detailed yaw angle and pitot pressure profiles in the two flows have different physical scales but similar qualitative

features. The two data sets can be correlated using an extension of a simple scaling technique developed originally for surface features.

3) Large yaw angles at a significant distance above the test surface occur upstream of the shock wave and develop conically in the spanwise direction. The origin of this region is in the vicinity of the fin leading edge/virtual origin.

4) Use of δ_0 as a guide to the vertical scale of the flowfield, even as a first approximation, may lead to serious error, particularly at spanwise stations far from the fin leading edge.

Acknowledgments

This study was supported by the U.S. Air Force Office of Scientific Research under Contract F49620-81-0018 monitored by Dr. J. Wilson. Discussions with Dr. G.S. Settles and Prof. S.M. Bogdonoff are gratefully acknowledged.

References

[1]Dolling, D.S. and Bogdonoff, S.M., "Upstream Influence in Sharp Fin-Induced Shock Wave Turbulent Boundary Layer Interaction," *AIAA Journal*, Vol. 21, Jan. 1983, pp. 143-145.

[2]Settles, G.S., Perkins, J.J., and Bogdonoff, S.M., "Upstream Influence Scaling of 2D and 3D Shock/Turbulent Boundary Layer Interactions at Compression Corners," *AIAA Journal*, Vol. 20, June 1982, pp. 782-789.

[3]Dolling, D.S. and Bogdonoff, S.M., "Upstream Influence Scaling of Sharp Fin-Induced Shock Wave Turbulent Boundary Layer Interactions," AIAA Paper 81-0336, Jan. 1981.

[4]Lu, F. and Settles, G.S., "Conical Similarity of Shock Boundary Layer Interactions Generated by Swept Fins," AIAA Paper 83-1756, July 1983.

[5]Lu, F., "An Experimental Study of 3D Shock/Boundary Layer Interactions Generated by Swept Fins," MSE Thesis, Princeton University, Jan. 1983.

[6]Oskam, B., Bogdonoff, S.M., and Vas, I.E., "Study of Three-Dimensional Flow Fields Generated by the Interaction of a Skewed Shock Wave with a Turbulent Boundary Layer," AFFDL TR 75-21, Feb. 1975.

[7]Oskam, B., "Three Dimensional Flowfields Generated by the Interaction of a Swept Shock with a Turbulent Boundary Layer," Princeton University, Gas Dynamics Laboratory Rept. 1313, Dec. 1976.

[8]McClure, W.B., "An Experimental Study into the Scaling of an Unswept Sharp Fin Generated Shock/Turbulent Boundary Layer Interaction," MSE Thesis (1597-T) Mechanical & Aerospace Engineering Department, Princeton University, Jan. 1983.

[9]McClure, W.B. and Dolling, D.S., "Flowfield Scaling in Sharp Fin-Induced Shock Wave Turbulent Boundary Layer Interaction," AIAA Paper 83-1754, July 1983.

[10]Settles, G.S. and Teng, H.-Y., "Flow Visualization of Separated 3-D Shock Wave/Turbulent Boundary Layer Interactions," *AIAA Journal*, Vol. 21, Mar. 1983, pp. 390-397.

[11]Settles, G.S., "An Experimental Study of Compressible Turbulent Boundary Layer Separation at High Reynolds Number," Ph.D. Thesis, Princeton University, Sept. 1975.

[12]Kubota, H., "Investigations of Three-Dimensional Shock Wave Boundary Layer Interactions," AFOSR-76-3006, Jan. 1980.

[13]McCabe, A., "A Study of Three-Dimensional Interactions Between Shock Waves and Turbulent Boundary Layers," Ph.D. Thesis, University of Manchester, Ind., Oct. 1963.

[14]Lowrie, B.W., "Cross-Flows Produced by the Interaction of a Swept Shock Wave with a Turbulent Boundary Layer," Ph.D. Thesis, Cambridge University, Dec. 1965.

[15]Peake, D.J., "The Three-Dimensional Interaction of a Swept Shock Wave with a Turbulent Boundary Layer and the Effects of Air Injection on Separation," Ph.D. Thesis, Carleton University, Ottawa, Canada, March 1975.

[16]Horstman, C.C. and Hung, C.M., "Computation of Three-Dimensional Turbulent Separated Flows at Supersonic Speeds," AIAA Paper 79-0002, Jan. 1979.

[17]Knight, D.D., "A Hybrid Explicit-Implicit Numerical Algorithm for the Three-Dimensional Compressible Navier-Stokes Equations," AIAA Paper 83-0223, Jan. 1983.